IEEE Access
Multidisciplinary | Rapid Review | Open Access Journal

Received March 4, 2020, accepted March 13, 2020, date of publication March 17, 2020, date of current version March 27, 2020.

Digital Object Identifier 10.1109/ACCESS.2020.2981498

Drive Current Calculation and Analysis of Permanent Magnet Spherical Motor Based on Torque Analytical Model and Particle Swarm Optimization

RUI ZHOU[1], (Member, IEEE), GUOLI LI[2], (Member, IEEE), QUNJING WANG[3], (Member, IEEE), JINGXIONG HE[1], AND TINGTING WANG[1]

[1]School of Electrical Engineering and Automation, Anhui University, Hefei 230601, China
[2]National Engineering Laboratory of Energy-Saving Motor and Control Technology, Anhui University, Hefei 230601, China
[3]Collaborative Innovation Center of Industrial Energy-Saving and Power Quality Control, Anhui University, Hefei 230601, China

Corresponding author: Rui Zhou (11007@ahu.edu.cn)

This work was supported by the Key Project of the China National Natural Science Foundation "Research on Key Basic Issues of Complex Motor System (under Grant 51637001)", and by the Anhui Natural Science Fund Project "Sensorless posture detection of PMSM based on inductance model (under Grant 1908085QE236)".

ABSTRACT In order to determine the currents required in different attitudes and torque target conditions, this paper proposes a calculation method for drive currents of permanent magnet spherical motors based on three-dimensional magnetic field, torque analytical model and optimization algorithm. Firstly, an electromagnetic torque analytical model base on equivalent surface currents of a permanent magnet and Lorentz force is proposed. The feasibility and accuracy are verified by comparing results with those by the finite element method. Then, an inverse calculation model of the motor drive current is built by combining the torque analytical model with the Particle Swarm Optimization (PSO) algorithm. At last, using the proposed drive current calculation model, the driving current characteristics of spherical motors under different energization strategies are compared and analyzed.

INDEX TERMS Permanent magnet spherical motor, analytical model, electromagnetic torque, drive current, particle swarm optimization.

I. INTRODUCTION

Due to the compact structure with flexible motion mode and no characteristics of motion error accumulation [1], [2], the spherical motor is especially suitable for installation or motion in small space and has broad engineering applications in the field of robot arms and joints. Among them, a permanent magnet spherical motor is the main object of current spherical motor research for its high energy density. Since the magnetic field and the motion mode are always spatially distributed in three-dimension, the spherical motor torque calculation is far more complicated than that of the conventional motor. At present, the spherical motor torque calculation is mainly through the finite element method (FEM) combining with machine learning to acquire a black-box or gray-box model [3]–[9]. However, the FEM process is very time consuming, plus the black-box model accuracy is greatly depends on the distribution of the sample points. No matter using weighted undirected graphs [10], direct magnetic field feedback [11], torque map [12], torque domain estimation [13], or stator spherical domain partitioning [14], the determination process of drive current is usually even more complicated than torque calculation.

In order to reduce the grey-box degree of torque model and improve the versatility of the energization strategy, this paper takes a 24/8 permanent magnet spherical motor as an example. A spatial magnetic field distribution expression of rectangular permanent magnet is derived. Superposition theorem is used to establish a 3D no-load magnetic field model of the motor. A calculation model of the electromagnetic torque is derived by analyzing Lorentz force of the stator coil received after energized. Then, combining Particle Swarm Optimization algorithm with the torque model, a reverse solution model of the permanent magnet spherical

The associate editor coordinating the review of this manuscript and approving it for publication was Kan Liu.

motor drive current is established by optimizing the stator coil currents according to the given output torques. At last this drive current calculation model is used to analyze the characteristics of drive currents under different energization strategies.

II. TORQUE CALCULATION MODEL FOR PERMANENT MAGNET SPHERICAL MOTOR

The structure of the permanent magnet spherical motor studied in this paper is shown in figure 1. According to the symmetrical structure, the torque generated by whichever coil can also be generated by coil at the symmetrical position of the spherical center. Therefore 24 stator coils are not distributed along the equatorial plane, but one around the equator and the other distributed at 30° south latitude of the sphere. The coils in each layer are spaced 30 degrees apart in longitude. This design is equivalent to eliminate the upper coils that are symmetrical to the coils at 30° south latitude, and makes the opening at the top of the stator enlarged, so the pitching range of the rotor is increased. The rotor is provided with 16 rectangular NdFeB permanent magnets along the equator. The magnetization direction and spatial position of each permanent magnet are in accordance with the Halbach regulation to form an 8-poles rotor magnetic field, as shown in figure 2.

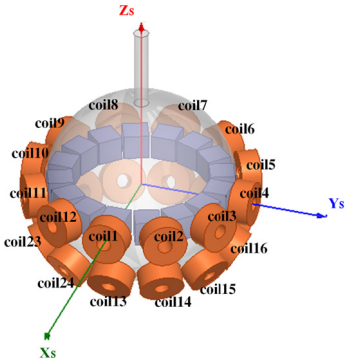

FIGURE 1. Distribution of Spherical motor stator coils and rotor magnets.

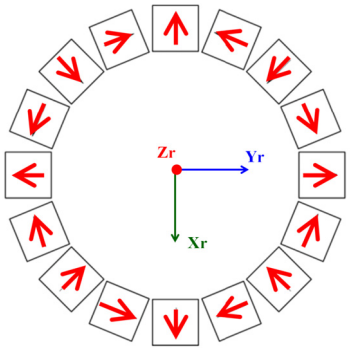

FIGURE 2. Magnetization direction of permanent magnets in rotor.

A. ANALYTICAL MODEL OF 3D MAGNETIC FIELD BASED ON EQUIVALENT SURFACE CURRENT OF RECTANGULAR PERMANENT MAGNET

According to the Ampere Circuital Theorem, the external magnetic field due to the uniformly magnetized permanent magnet is determined only by the bound surface currents on the side surface parallel to the magnetization direction [15], [16]. Take the rectangular permanent magnet shown in figure 3 as example. The origin of the orthogonal coordinate system is placed at the center of the permanent magnet. The length, width and height of the permanent magnet are marked as L_x, L_y, and L_z, and the magnetization direction is along the Z-axis direction. The permanent magnet can be equivalent to the surface currents on the four sides parallel to the Z-axis, in accordance with the right-handed spiral relationship. The density I of the surface current in the magnetization direction is exactly the magnetization intensity H_c of the permanent magnet. Br in (1) is the permanent magnet residual magnetization and this paper takes *1.2T* for calculation. $\mu_0 = 4\pi \times 10^{-7}\ H/m$ is the vacuum permeability.

$$I = \frac{B_r}{\mu_0} = H_c \tag{1}$$

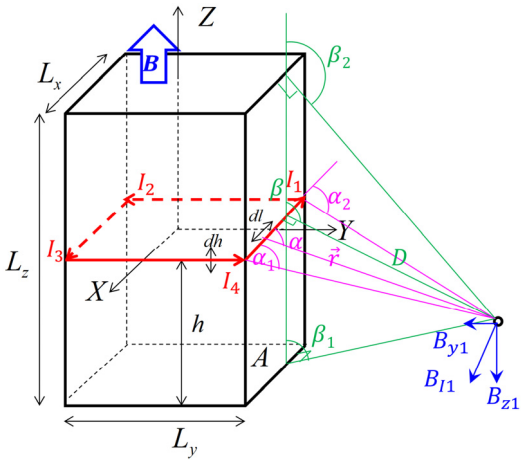

FIGURE 3. Surface current model of rectangular permanent magnet.

According to the calculation method of the magnetic induction intensity at a certain point on a plane by a straight current-carrying wire, divide the rectangular permanent magnet into a series of slices with thickness of *dh* perpendicular to the magnetization direction. The currents $I_1 \sim I_4$ at the four edges of every slice are *Idh*. The magnetic induction generated in space by each magnet slice can be regarded as a superposition effects of $I_1 \sim I_4$ excitation. Correspondingly, the magnetic density of the whole permanent magnet can be regarded as accumulation of excitation effects by all the edge currents of all the magnet slices. Take B_{I1} as calculation target, which is generated at point *P(x, y, z)* by I_1 in the negative direction of the X-axis on the edge of a magnet slice at height $z = h$. Mark the vertical line from point I_1 to *P* as *D*.

The direction of B_{I1} is perpendicular to D and corresponds to the right-handed rule with I_1. Suppose there is a current element $I_1 dl$ within I_1, then the angle is α between the line connecting the $I_1 dl$ with point P and I_1. As the movement of $I_1 dl$ from the start point of I_1 to the end point, α changes from α_1 to α_2. Assume that the vector from $I_1 dl$ to P is r, and according to Biot-Savar's law [17],

$$dB_{I1} = \frac{\mu_0}{4\pi}\frac{\vec{Idl}\times\vec{r}}{r^3} = \frac{\mu_0}{4\pi}\frac{Idl\cdot\sin\alpha}{r^2}. \tag{2}$$

From figure 3:

$$\begin{cases} l = r\cos(\pi-\alpha) \\ D = r\sin(\pi-\alpha) \end{cases} \Rightarrow \frac{l}{D} = -\cot\alpha \Rightarrow dl = \frac{D}{\sin^2\alpha}d\alpha. \tag{3}$$

l is the distance between dl and D's foot of perpendicular, and it takes the direction of I1 as the positive direction. Take integral in the range of α_1 to α_2:

$$\begin{aligned} B_{I1} &= \int_{\alpha_1}^{\alpha_2}\frac{\mu_0 I_1}{4\pi}\frac{\sin^2\alpha}{D^2}\frac{D}{\sin^2\alpha}\sin\alpha d\alpha \\ &= \frac{\mu_0 I_1}{4\pi D}(\cos\alpha_1 - \cos\alpha_2). \end{aligned} \tag{4}$$

(4) is the scalar value of the magnetic induction intensity generated at point P by the edge current of the magnet slice with a thickness of dh at the height $z = h$. The angle between the vertical line D from point P to I_1 and the Z axis is denoted by β. Integrating the thickness dh in the Z-direction and considering the right-handed spiral relationship of B_{I1} and I_1, the 3D magnetic-density by I_1 at point P in the range of $\beta \geq 0$ or $y \geq Ly/2$ can be obtained as

$$\begin{cases} B_{x1} = 0 \\ B_{y1} = \int_{\beta_1}^{\beta_2}\frac{\mu_0 I}{4\pi D}(\cos\alpha_1 - \cos\alpha_2)\cos\beta dh \\ B_{z1} = -\int_{\beta_1}^{\beta_2}\frac{\mu_0 I}{4\pi D}(\cos\alpha_1 - \cos\alpha_2)\sin\beta dh. \end{cases} \tag{5}$$

From the geometric relationship in figure 3, following can be obtained:

$$\begin{cases} D = \dfrac{y - L_y/2}{\sin\beta} \Rightarrow \begin{cases} \alpha_1 = \arctan(\dfrac{1}{\sin\beta}\dfrac{y-L_y/2}{L_x/2-x}) \\ \alpha_2 = \arctan(\dfrac{1}{\sin\beta}\dfrac{y-L_y/2}{-L_x/2-x}) \end{cases} \\ \dfrac{h}{y-L_y/2} = -\cot\beta \Rightarrow dh = \dfrac{y-L_y/2}{\sin^2\beta}d\beta. \end{cases} \tag{6}$$

By replace α in (5), the following is obtained:

$$\begin{cases} B_{x1} = 0 \\ B_{y1} = \dfrac{\mu_0 I_1}{4\pi}\displaystyle\int_{\beta_1}^{\beta_2} \begin{matrix} \{\cos[\arctan(\frac{1}{\sin\beta}\frac{y-L_y/2}{L_x/2-x})] \\ -\cos[\arctan(\frac{1}{\sin\beta}\frac{y-L_y/2}{-L_x/2-x})]\} \\ \cot\beta d\beta \end{matrix} \\ B_{z1} = -\dfrac{\mu_0 I_1}{4\pi}\displaystyle\int_{\beta_1}^{\beta_2} \begin{matrix} \{\cos[\arctan(\frac{1}{\sin\beta}\frac{y-L_y/2}{L_x/2-x})] \\ -\cos[\arctan(\frac{1}{\sin\beta}\frac{y-L_y/2}{-L_x/2-x})]\} \end{matrix} d\beta. \end{cases} \tag{7}$$

(7) is the analytical expression of the magnetic induction intensity generated at P by the equivalent currents on magnet surface A shown in figure 3, where β_1 and β_2 are calculated by inverse tangent function according to the size of the magnet and the coordinates of point P. Similarly, the magnetic induction density components generated by the equivalent currents on the other three faces of the magnet can be calculated. By Combining with the superposition theorem, the analytical model of the spatial magnetic induction density of the whole rectangular permanent magnet can be obtained. Furthermore, for the synthesis of the magnetic field of multiple permanent magnets, due to the different spatial position distributions and magnetization directions, the coordinates of the observation point P in global coordinate system as shown in figure 2 needs to be translated and rotated to obtain the coordinates of P in relative coordinate system of each magnet and calculate the magnetic density value generated by each magnet according to this relative coordinate value. Then these series of magnetic density values are projected back to the global coordinate system, and accumulated according to the superposition theorem to obtain the 3D magnetic density components generated by the entire rotor at the observation point P.

For the specific magnetic field of Halbach array permanent magnets in the spherical motor studied in this paper as shown in figure 1 & 2, the distance is 48mm between the bottom surface of each magnet and the center of the sphere. The length, width and height of each magnet are 17mm. 16 rectangular magnets are spaced by 22.5° along the equator. Using the analytical method proposed above and the FEM, the orthogonal magnetic densities on a 180° equatorial arc are calculated and shown in figure 4. It can be seen that the results of the analytical calculation are basically consistent with that of the FEM, which means the analytical model of the magnetic field can be used as the basis for calculating the motor torque later. Usually, the analysis of the magnetic field of the motor is aimed at radial magnetic density. However, for the calculation of the torques of the spherical motor, the orthogonal magnetic densities are more convenient than the radial magnetic density. Therefore, the orthogonal magnetic densities are not synthesized into the radial magnetic density here.

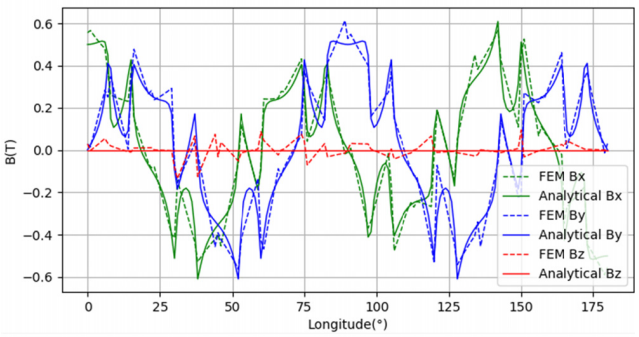

FIGURE 4. 3D magnetic density of the rotor.

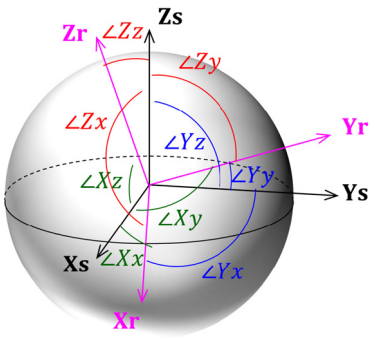

FIGURE 5. Angles between the stator and the rotor coordinate system.

B. ANALYTICAL MODEL OF MOTOR TORQUE BASED ON LORENTZ FORCE

According to the basic principles of engineering mechanic and electromagnetics, the coil in the rotor's magnetic field will generate Lorentz force when it carries current. The torque generated by Lorentz force of the coil around the sphere center has the same value and reverse direction with the torque of the rotor. Therefore, in this paper, firstly it is calculated the coordinate position of the coil current element in the rotating coordinate system of the rotor. Secondly the magnetic densities in the rotor coordinate are calculated by using the magnetic field analytical model established in the previous section. Then, according to the rotational relationship between the stator stationary and the rotor rotating coordinate system, the magnetic density obtained in the rotor system is projected back to the stator system. At last, the Lorentz force is calculated, which is received by the stationary coil with those magnetic densities in stator system. Together with the length of the rotating radius, the electromagnetic torque generated in the rotor can be obtained. After the rotor rotation, the space relationship and angle definitions between axes of two coordinate systems are as shown in figure 5. The magnetic density components B_{xr}, B_{yr}, and B_{zr} in the rotor coordinate system are projected to the stator coordinate system into B_{xs}, B_{ys}, B_{zs} by (8). The nine angles can be calculated from the cosine theorem according to the unit vector of the stator and rotor coordinate axes.

$$\begin{bmatrix} B_{xs} \\ B_{ys} \\ B_{zs} \end{bmatrix} = \begin{bmatrix} \cos\angle Xx & \cos\angle Xy & \cos\angle Xz \\ \cos\angle Yx & \cos\angle Yy & \cos\angle Yz \\ \cos\angle Zx & \cos\angle Zy & \cos\angle Zz \end{bmatrix} \begin{bmatrix} B_{xr} \\ B_{yr} \\ B_{zr} \end{bmatrix}. \quad (8)$$

In direction setting of the stator stationary coordinates as shown in figure 1, according to the integral form of Lorentz force [18], the following can be obtained:

$$\begin{aligned} \vec{F} &= \int_v \vec{f}\, dv = \int_v \vec{J} \times \vec{B} dv \\ &= \int_v \begin{vmatrix} x & y & z \\ J_x & J_y & J_z \\ B_{xs} & B_{ys} & B_{zs} \end{vmatrix} dv \Rightarrow \begin{cases} f_x = J_y \cdot B_{zs} - J_z \cdot B_{ys} \\ f_y = J_z \cdot B_{xs} - J_x \cdot B_{zs} \\ f_z = J_x \cdot B_{ys} - J_y \cdot B_{xs}. \end{cases} \end{aligned} \quad (9)$$

Assume that all currents in the coil flow through a circular path perpendicular to the coil axis. The geometric model of the current element J in the stator coordinate system is shown in figure 6. Mark the angle between the coil axis and the $XsOYs$ plane of the stator coordinate system as the latitude angle lat, and the angle between the coil axis projection on the $XsOYs$ plane and the Xs axis as the longitude angle lon. Denote the radius of the route as R where the current element is located. The angle between R and the projection of the Zs axis on the current route plane is denoted as θ. According to the geometric relationship shown in figure 6, the current elements can be expressed as (10), and the coordinates of current elements in the stator stationary system can be expressed as (11):

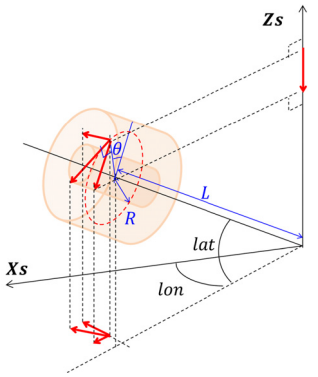

FIGURE 6. The model of coil current element components.

$$\begin{cases} J_x = J(\sin\theta \cdot \sin lat \cdot \cos lon + \cos\theta \cdot \sin lon) \\ J_y = J(\sin\theta \cdot \sin lat \cdot \sin lon - \cos\theta \cdot \cos lon) \\ J_z = -J \cdot \sin\theta \cdot \cos lat, \end{cases} \quad (10)$$

$$\begin{cases} xr = (L \cdot \cos lat - R \cdot \cos\theta \cdot \sin lat)\cos lon \\ \quad +R \cdot \sin\theta \cdot \sin lon \\ yr = (L \cdot \cos lat - R \cdot \cos\theta \cdot \sin lat)\sin lon \\ \quad -R \cdot \sin\theta \cdot \cos lon \\ zr = L \cdot \sin lat + R \cdot \cos\theta \cdot \cos lat. \end{cases} \quad (11)$$

By considering the reaction relationship between coil torque and rotor torque and integrating the product of the Lorentz force and the arm of force over the entire coil volume,

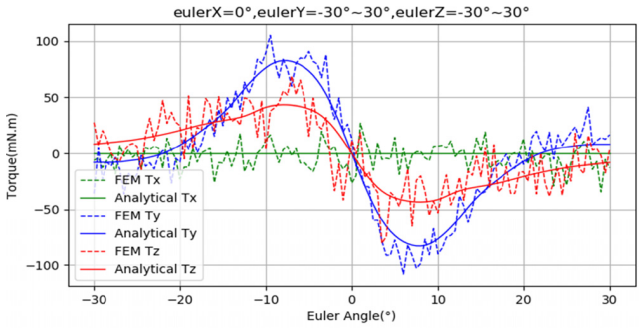

FIGURE 7. Single coil torque comparison.

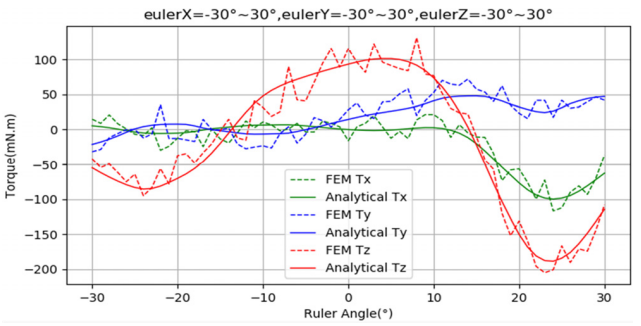

FIGURE 8. Multi-coils torque comparison.

the spherical motor rotor torque is obtained as below:

$$\begin{cases} T_x = \int_v (f_y \cdot z - f_z \cdot y) dv \\ T_y = \int_v (f_z \cdot x - f_x \cdot z) dv \\ T_z = \int_v (f_x \cdot y - f_y \cdot x) dv. \end{cases} \tag{12}$$

(8), (9), (10) and (12) together is the analytical model for electromagnetic torque by energizing single coil. According to the superposition principle of force, the electromagnetic torque of the whole motor can be obtained by accumulating the torques generated by each coil at different latitude and longitude separately. For the specific spherical motor studied in this paper, the distribution of 24 coils is shown in figure 1. The distance between the coil and the center of the sphere is 66.5 mm, the stack height of the coil is 13.5 mm, the inner/outer diameter is 10/30 mm, and the number of turns is 500. The following two examples are used to verify the validity of the proposed torque model.

(A) Apply 1A counterclockwise DC to a single coil at E0°N0°. Assume that the X-axis rotation Euler angle of the rotor maintains zero, and Y and Z-axis Euler angles spin from −30° to 30° synchronously. The comparison between the analytical results and the FEM results is shown in figure 7. The analytical calculation takes about ten seconds, and the FEM calculation takes dozens of minutes. Since there is no rotation around the X-axis, T_x remains zero. There are more magnets distributed along the latitude than those along the longitude, so the sign invariant part of T_z waveform is wider than that of the T_y waveform. At the point the three Euler angles are all zero, since the energized coil is in a straight line with a N pole of the rotor, the radial force reaches its maximum while the tangential force is minimum. So the torques on all three axes are zeros. The situations shown in figure 7 are in full compliance with the above predictions.

(B) Apply 1A DC to the coil at E30°N0° and 2A DC with the same direction to the coil at E0°S30°. Spin the three Euler angles synchronously from −30° to 30°. The comparison between the analytical results and the FEM analysis results is shown in figure 8. The analytical torques are calculated by accumulating the torque generated by each coil. The waveform shown in figure 8 verifies the feasibility of the superposition principle for the rotor torque.

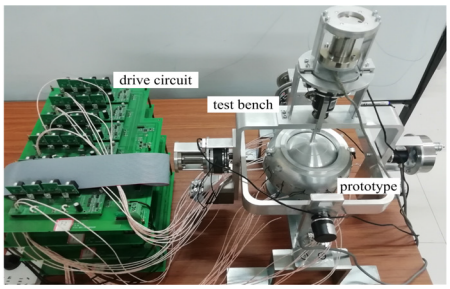

FIGURE 9. Experimental platform.

In order to verify the method proposed, an experimental platform is built, as shown in figure 9. The platform consists of three main parts: the prototype, the drive circuit, and the test bench. The main dimensions of the prototype are as described above. The driving circuit adopts STM32 digital chip to control 24 independent DC controllable outputs. Each current source is composed of a constant current source circuit powered by a 24V DC power supply. The test bench consists of a stationary bracket and two rotating brackets, each equipped with a rotary encoder and a torque sensor. The data collected by the sensor is transmitted to the host computer by RS485 protocol.

Verify the result of example A. In order to reduce the influence of interference factors such as friction, the current in coil at E0°N0° is enlarged by three times, theoretically the torque should also be increased by three times. The test results are shown in figure 10. Then verify the result of example B. The two coil currents are both doubled, theoretically the torques should also be doubled too. The test results are shown in figure 11. It can be seen that due to the friction and other factors, the calculated torques are higher than the actual test torques. However, on the trend, the calculation result of the torque curve is basically consistent with the actual output, so it can be confirmed that the proposed torque calculation model is accurate and effective.

III. CALCULATION MODEL OF DRIVE CURRENTS BASED OF PERMANENT MAGNET SPHERICAL MOTOR ON PSO

The drive currents that need to be applied to all stator coils for a given posture and target torques are more important than the

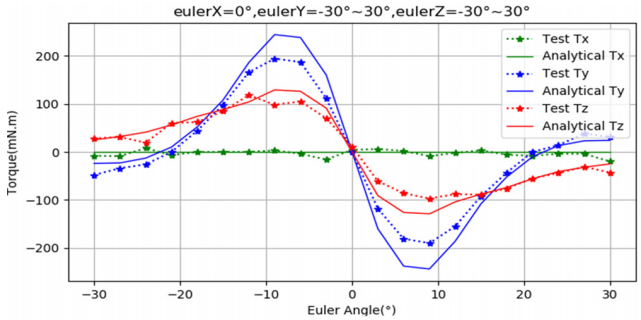

FIGURE 10. Experimental (A).

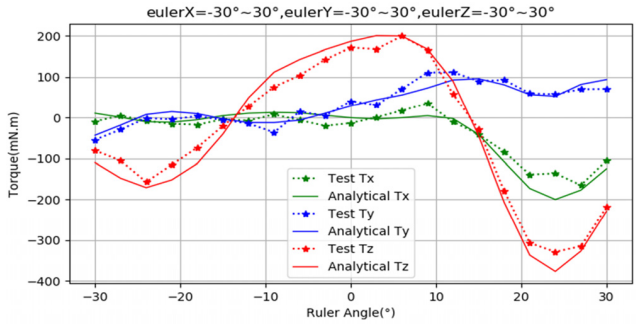

FIGURE 11. Experimental (B).

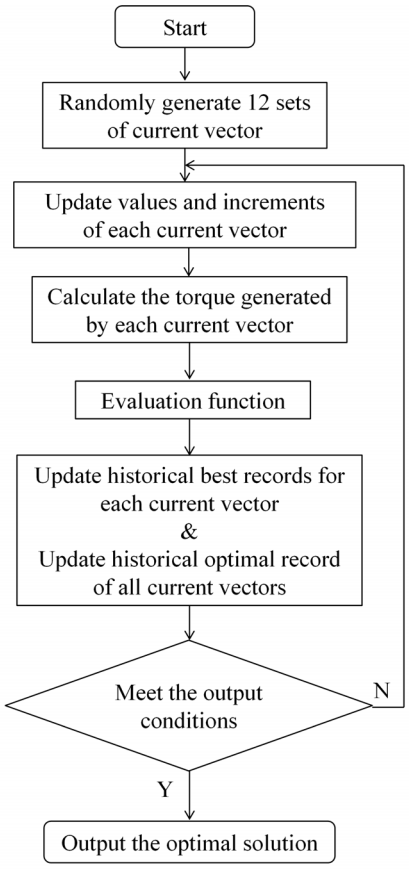

FIGURE 12. Calculation process of drive currents.

electromagnetic torque of a spherical motor. Because of the redundancy in the design of the permanent magnets and coils, this current solution is usually not unique.

This study uses the torque analysis model proposed in the previous section combining with Particle Swarm Optimization (PSO) algorithm, and sets the output torques and other additional conditions as the output conditions. The drive currents of all coils are set as the optimization target. The flow chart of the calculation model is shown in figure 12. The main parameters of the algorithm are given below. The number of particles is set to 12, the dimensions of the particle is 24 according to the number of coils, the speed constants c_1 and c_2 are equal to 2, and the range of the current of each coil is $-3\sim3$A. The evaluation function and the termination condition need to be constructed according to different energization strategies.

IV. COMPARISON AND ANALYSIS OF ENERGIZATION STRATEGIES

For the spherical motor energization strategy, the prime thing is to meet the electromagnetic torque demand under certain posture and operating condition. On this basis, it is also desirable to reduce the number and amount of currents that the coils carry, hence to reduce the burden of power source, communication, etc. This section assumes that the rotor is in the posture with Euler angles sequence and sizes of $\mathrm{X10}^\circ - \mathrm{Y20}^\circ - \mathrm{Z30}^\circ$. When the target torque is: $T_x = 0$, $T_y = 100mNm$, $T_z = 200mNm$, the following three different energization strategies are compared. The numbering rule of the coil and current are shown in figure 1.

A. TORQUE DOMINANT STRATEGY

This strategy only satisfies the torque demand, and the number of energized coils and the total current load are not considered. Accordingly, the evaluation function is constructed as (13). *Txg*, *Tyg*, and *Tzg* are the goal values of torques, used as the optimization goals by PSO. Different from genetic algorithm selecting the parent individuals according to the probability proportional of the fitness level, PSO algorithm can filter the best individual based on the minimum fitness. The aim of (13) is to calculate the maximum value of the differences between the 3-Dof torque target values and the calculated values, which is used as a criterion for judging the individual in the swarm. Obviously with this setting, the fitness of the ideal optimal solution is zero. Thus the optimal individual should be found according to the minimum value. The calculation results are shown in Table 1. Since the target value of T_x is 0, the bias percentage of T_x is not given.

$$evaluation_A = \max(\left\| T_x - T_{xg} \right\|, \left\| T_y - T_{yg} \right\|, \left\| T_z - T_{zg} \right\|). \tag{13}$$

The results show that the calculated drive currents can produce sufficiently accurate electromagnetic torques.

TABLE 1. Calculation results for drive current strategy (A).

I_1(A)	I_2(A)	I_3(A)	I_4(A)	I_5(A)	I_6(A)	I_7(A)	I_8(A)
3.000	-3.000	-3.000	-3.000	3.000	-2.012	3.000	3.000
I_9(A)	I_{10}(A)	I_{11}(A)	I_{12}(A)	I_{13}(A)	I_{14}(A)	I_{15}(A)	I_{16}(A)
3.000	-3.000	-3.000	-3.000	3.000	3.000	-2.259	3.000
I_{17}(A)	I_{18}(A)	I_{19}(A)	I_{20}(A)	I_{21}(A)	I_{22}(A)	I_{23}(A)	I_{24}(A)
-3.000	-3.000	-0.171	2.435	-3.000	3.000	0.566	-3.000
T_x(mNm)		T_y(mNm) /bias		T_z(mNm) /bias		I_{RMS}(A)	
-1.168		98.211/-1.8%		196.736/-1.6%		2.79	

TABLE 2. Calculation results for drive current strategy (B).

I_1(A)	I_2(A)	I_3(A)	I_4(A)	I_5(A)	I_6(A)	I_7(A)	I_8(A)
-1.700	0.152	0.147	-0.879	3.000	-0.113	1.095	0.663
I_9(A)	I_{10}(A)	I_{11}(A)	I_{12}(A)	I_{13}(A)	I_{14}(A)	I_{15}(A)	I_{16}(A)
1.376	-1.304	-3.000	-3.000	0.215	0.850	0.313	0.743
I_{17}(A)	I_{18}(A)	I_{19}(A)	I_{20}(A)	I_{21}(A)	I_{22}(A)	I_{23}(A)	I_{24}(A)
-0.721	0.212	-3.000	3.000	2.698	-3.000	0.518	-1.272
T_x(mNm)		T_y(mNm) /bias		T_z(mNm) /bias		I_{RMS}(A)	
-5.077		100.436/+0.4%		199.149/-0.4%		1.76/(-36.9%)	

However, from the symmetry of the coil positions in the magnetic field in figure 1, the driving effects of all upper layer coils can be replaced or neutralized by a coil at the symmetry of the spherical center. As shown in Table 1, both I_1 and I_7 are 3A. In case of the power source allowed, a 6A current can be applied to coil 1 or coil 7 instead of 3A current each. The same rule is suitable for I_4 and I_{10}, I_6 and I_{12}. On the other hand, the driving effects of I_2 and I_8 are mutually offset, which means no current is needed for any of these two coils. The same holds true for current pairs I_3 and I_9, I_5 and I_{11}. It can be seen that the energization strategy that merely satisfies the torque requirements will bring unnecessary burden to the power source and the controller. Therefore, two improvement strategies are proposed below. In order to compare the improvement, Table 1 gives the root mean square (RMS) of all coil currents.

B. STRATEGY OF GUARANTEED TORQUE AND MINIMUM SUM OF CURRENTS

This strategy limits the total currents of the coils while satisfying the torque demands. The total current is measured by the RMS of currents, and the evaluation function is constructed as (14). The aim of (14) is control the algorithm search direction to minimize torque biases and minimize the RMS of currents at the same time. The calculation results are shown in Table 2.

$$evaluation_B = \max(\left\|T_x - T_{xg}\right\|, \left\|T_y - T_{yg}\right\|, \left\|T_z - T_{zg}\right\|) \cdot (1 + \sqrt{\frac{1}{24}\sum_{i=1}^{24} I_i^2}) \quad (14)$$

In Table 2, although neutralized currents, such as I_1 and I_7, I_5 and I_{11}, still exist, the RMS value of total currents load RMS decreases from 2.79A to 1.76A by a drop of 36.9%.

TABLE 3. Calculation results for drive current strategy (C).

I_1(A)	I_2(A)	I_3(A)	I_4(A)	I_5(A)	I_6(A)	I_7(A)	I_8(A)
1.602	0.000	0.000	0.000	0.070	0.795	0.145	-0.893
I_9(A)	I_{10}(A)	I_{11}(A)	I_{12}(A)	I_{13}(A)	I_{14}(A)	I_{15}(A)	I_{16}(A)
1.164	0.026	0.000	1.027	-3.000	-0.390	-3.000	2.352
I_{17}(A)	I_{18}(A)	I_{19}(A)	I_{20}(A)	I_{21}(A)	I_{22}(A)	I_{23}(A)	I_{24}(A)
2.062	-2.061	-2.578	0.189	3.000	1.877	-0.836	0.730
T_x(mNm)		T_y(mNm) /bias		T_z(mNm) /bias		I_{RMS}(A)	
1.042		99.402/0.6%		197.915/1.0%		1.57(-43.7%)	

C. STRATEGY OF GUARANTEED TORQUE AND LEAST ENERGIZED COILS

Under the premise of satisfying the torque demands, this strategy reduces the number of energized coils as many as possible, and the evaluation function is constructed as shown in (15). The aim of equation (15) is control the algorithm search direction to minimize torque biases and minimize the number of currents at the same time. At the same time, the code to avoid the occurrence of torque mutual offset is added for $I_1 \sim I_{12}$. The calculation results are shown in Table 3.

$$\begin{cases} evaluation_C = \dfrac{(T_x - T_{xg})^2 + (T_y - T_{yg})^2 + (T_z - T_{zg})^2}{1 + \sum_{i=1}^{24} N_i} \\ N_i = \begin{cases} 1, & I_i \neq 0 \\ 0, & I_i = 0. \end{cases} \end{cases} \quad (15)$$

From Table 3, I_2, I_3, I_4, and I_{11} are zero, indicating neutralized current is no longer existing, and the goal of reducing the energized coils number is achieved. Since the occurrence of ineffective current is avoided, the RMS value of the total current is reduced from 2.79A to 1.57A, which is reduced by 43.7%.

V. CONCLUSION

In this paper, the spatial magnetic field distribution expression of rectangular permanent magnet is deduced firstly. Then a 3D analytical model of the rotor magnetic field of spherical motor is established using the superposition theorem. Based on this magnetic field model, Lorentz force integral method is used to establish a 3D analytical model of electromagnetic torque. After that, the PSO algorithm is combined with the torque model to construct a reverse solution model for drive currents of the permanent magnet spherical motor. By comparing the FEM and analytical results of magnetic field and torque and comparing the drive currents under different energization strategies, the following conclusions are drawn:

(1) The equivalent surface current model can accurately calculate the spatial magnetic density of the permanent magnet. Under the premise of no nonlinear ferromagnetic material, using the superposition method can effectively calculate the synthetic magnetic field of multiple permanent magnets;

(2) By calculating the Lorentz force of the stator coil to reckon the force of the rotor according to the reaction

principle, the rotor torque can be effectively calculated. The torque generated by multiple coils can be obtained by the accumulation of torque from each coil;

(3) By combine the torque calculation with the optimization algorithm, the drive currents with arbitrary torque within the allowable range can be calculated. Redundancy may exist in the current solution and can be controlled by designing a reasonable evaluation function and termination condition.

REFERENCES

[1] W. Qun-Jing, L. Zheng, and X. Kun, "Calculation and analysis on configuration parameters and torque characteristics of a novel spherical stepper motor," *Proc. CSEE*, vol. 26, no. 10, pp. 158–165, 2006.

[2] L. Zheng, L. Qingqing, and X. Zhengtao, "Calculation and analysis of magnetic field and Torque characteristics for 3-DOF deflection type PM motor," *Trans. China Electrotech. Soc.*, vol. 32, no. 23, pp. 81–90, 2017.

[3] L. Ju, Q. Wang, Z. Qian, A. Wang, and J. Liu, "Modeling and optimization of spherical motor based on support vector machine and chaos," in *Proc. Int. Conf. Electr. Mach. Syst.*, Tokyo, Japan, Nov. 2009, pp. 1–4.

[4] Z. Qian, Q. Wang, L. Ju, A. Wang, and J. Liu, "Torque modeling and control algorithm of a permanent magnetic spherical motor," in *Proc. Int. Conf. Electr. Mach. Syst.*, Tokyo, Japan, Nov. 2009, pp. 1–6.

[5] Z. Li and S. Li, "Electromagnetic system modeling and analysis of a 3-DOF type combined drive motor," in *Proc. IEEE 11th Conf. Ind. Electron. Appl. (ICIEA)*, Jun. 2016, pp. 1305–1310.

[6] S. Li, "Electromagnetic analysis and structure optimzaion of a vovel 3-DoF compound drive type motor," Ph.D. dissertation, School Elect. Eng., Hebei Univ. Sci. Technol., Shijiazhuang, China, 2017.

[7] L. Zheng, Z. Lu, W. Qunjing, and L. Qingqing, "Optimal design of structure parameters of three-dof deflection type PM motor based on response surface methodology," *Trans. China Electrotech.Soc.*, vol. 30, no. 13, pp. 134–142, 2015.

[8] W. Yaling, X. Yanliang, and L. Xiquan, "Dual-stator permanent magnet synchronous generator (I)—Schematic structure and design based on response surface method," *Trans. China Electrotech. Soc.*, vol. 26, no. 7, pp. 167–172, Jun. 2011.

[9] L. Ren, R. Chen, H. Xia, and Z. Ding, "An omni-directional kinetic energy harvester using a novel spherical Halbach array transducer," *Int. J. Appl. Electromagn. Mech.*, vol. 54, no. 2, pp. 249–262, May 2017.

[10] W. Qunjing, C. Lixia, and W. Lijian, "The control OFA permanent magnet spherical stepper motor based on weighted graph," *Proc. CSEE*, vol. 25, no. 9, pp. 130–134, May 2005.

[11] K. Bai and K.-M. Lee, "Direct field-feedback control of a Ball-Joint-Like permanent-magnet spherical motor," *IEEE/ASME Trans. Mechatronics*, vol. 19, no. 3, pp. 975–986, Jun. 2014.

[12] A. Gofuku, Y. Yamamoto, T. Yano, and N. Kasashima, "Driving technique of electromagnets to rotate spherical motors based on torque map," in *Proc. Int. Symp. Power Electron., Electr. Drives, Autom. Motion (SPEEDAM)*, Jun. 2016, pp. 861–865.

[13] K. Takahara, K. Hirata, N. Niguchi, Y. Nishiura, and Y. Sakaidani, "Evaluation method for Multidegree-of-Freedom spherical actuators under power control," *IEEE Trans. Magn.*, vol. 53, no. 11, pp. 1–5, Nov. 2017.

[14] C. Xia, C. Guo, and T. Shi, "A neural-network-identifier and fuzzy-controller-based algorithm for dynamic decoupling control of permanent-magnet spherical motor," *IEEE Trans. Ind. Electron.*, vol. 57, no. 8, pp. 2868–2878, Aug. 2010.

[15] K.-M. Lee and H. Son, "Distributed multipole model for design of Permanent-Magnet-Based actuators," *IEEE Trans. Magn.*, vol. 43, no. 10, pp. 3904–3913, Oct. 2007.

[16] H. Rezaei and S. Vaez-Zadeh, "Modelling and analysis of permanent magnet electrodynamic suspension systems," *Prog. Electromagn. Res. M*, vol. 36, pp. 77–84, May 2014.

[17] S. Song, B. Li, W. Qiao, C. Hu, H. Ren, H. Yu, Q. Zhang, M. Q.-H. Meng, and G. Xu, "6-D magnetic localization and orientation method for an annular magnet based on a closed-form analytical model," *IEEE Trans. Magn.*, vol. 50, no. 9, Sep. 2014, Art. no. 5000411.

[18] C. Xia, H. Li, and T. Shi, "3-D magnetic field and torque analysis of a novel Halbach array permanent-magnet spherical motor," *IEEE Trans. Magn.*, vol. 44, no. 8, pp. 2016–2020, Aug. 2008.

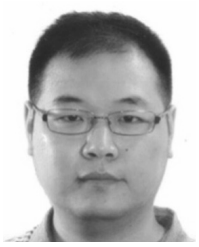

RUI ZHOU (Member, IEEE) received the B.S. degree in mechanical and electrical engineering from Anhui Jianzhu University, in 2008, and the M.S. degree in electric machines and electric apparatus from the Hefei University of Technology, in 2011. He is currently pursuing the Ph.D. degree in computer science and technology, Anhui University.

His researches focus on the fields of spherical motor drive and algorithm design.

GUOLI LI (Member, IEEE) received the B.Eng. and M.S. degrees in electrical engineering from the Hefei University of Technology, Hefei, China, in 1983 and 1987, respectively, and the Ph.D. degree in nuclear energy science and engineering from the Hefei Institute of Physical Sciences, Chinese Academy of Sciences, Hefei, in 2006.

She was a Lecturer, from 1983 to 1997, an Associate Professor, from 1997 to 2002, and a Professor, from 2002 to 2007, with the Hefei University of Technology. From 2007 to 2010, she was a Professor with the Zhejiang University of Technology, Hangzhou, China. Since 2010, she has been a Professor with Anhui University, Hefei. Her research interests include motor optimization and robotics.

QUNJING WANG (Member, IEEE) received the Ph.D. degree in precision instrument and machinery from the University of Science and Technology of China (USTC), Hefei, China, in 1998.

From 1983 to 2007, he was with the Hefei University of Technology, Hefei. Since 2007, he has been a Professor and the Vice-President with Anhui University, Hefei. He is currently a Research Chair Professor with the National Engineering Laboratory of Energy-Saving Motor and Control Technique, the Power Quality Engineering Research Centre of China Ministry of Education, and the Provincial Collaborative Innovation Centre of Industrial Energy-Saving and Power Quality Control, Anhui University. His research interests include motor and drive, converter technology, power quality, and micro grids.

JINGXIONG HE was born in Anqing, China, in 1995. He received the B.Eng. degree in electrical engineering from Anhui University (AHU), Hefei, China, in 2017, where he is currently pursuing the M.Eng. degree in electrical engineering with the School of Electrical Engineering and Automation.

His current research interests include the optimization design and torque measurement of special electric machines.

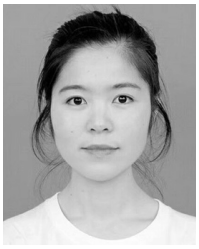

TINGTING WANG received the bachelor's degree in electrical engineering and automation from Suzhou University, Suzhou, China, in 2018. She is currently pursuing the master's degree with Anhui University. Her research interest includes permanent magnet spherical motor.